Controlling the Fate of Protein Corona by Tuning Surface Properties of Nanoparticles

ARTICLE *in* JOURNAL OF PHYSICAL CHEMISTRY LETTERS · OCTOBER 2013

Impact Factor: 7.46 · DOI: 10.1021/jz401874u

3 AUTHORS, INCLUDING:

Abhishek Gupta
Indian Institute of Technology Mandi
13 PUBLICATIONS **29** CITATIONS
SEE PROFILE

Chayan K Nandi
Indian Institute of Technology Mandi
33 PUBLICATIONS **204** CITATIONS
SEE PROFILE

THE JOURNAL OF PHYSICAL CHEMISTRY Letters

Letter

pubs.acs.org/JPCL

Controlling the Fate of Protein Corona by Tuning Surface Properties of Nanoparticles

Syamantak Khan, Abhishek Gupta, and Chayan Kanti Nandi*

School of Basic Sciences, Indian Institute of Technology Mandi, Himachal Pradesh, India 175001

Supporting Information

ABSTRACT: In a biological environment, the formation of a protein layer (protein corona) around nanoparticles immensely hampers its targeting capabilities and efficiency of specific delivery. Rational design of a nanoparticle remains one of the biggest challenges due to the lack of in-depth knowledge of the molecular mechanism of this corona formation on the different nanoparticle surfaces. Using computer simulation and experimental study, here, we establish for the first time the role of different surface properties like charge, chain length, architecture, and surface density of different surfactant molecules in the formation of the protein corona. We provide insights into the nanoparticle protein interaction, especially with respect to the structural orientation of a particular protein (human serum albumin) around a gold nanoparticle. We also derived the theoretical optimal conditions to avoid this corona formation. Such an efficient approach can pave the way to engineer smarter nanoparticles, which will avoid the protein absorption to keep their original properties unchanged.

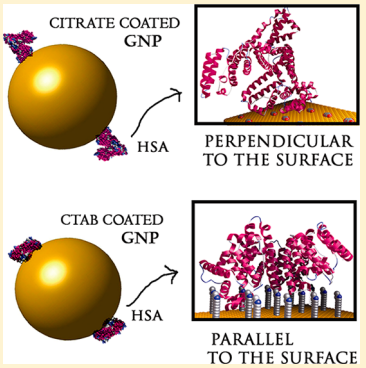

SECTION: Physical Processes in Nanomaterials and Nanostructures

The chemistry of ligands around gold nanoparticles (GNPs) plays a crucial role for their different biological activities, for example, cellular uptake, internal localization, cell penetration, as well as the influence in cellular response and cell proliferation.[1−8] Various anisotropic GNPs like gold nanorods, prisms, cages, and cubes, which are of great importance because of their different shapes and crystal facets, are primarily stabilized by cetyltrimethyl ammonium bromide (CTAB) in the synthesis process.[9−12] However, CTAB-coated GNPs are toxic in nature.[1,13] Hence, to reduce the cytotoxicity level of these anisotropic GNPs, CTAB is exchanged by mercapto acids, PEGylated molecules, polyethylene oxide, and other polymer-coated nontoxic capping agents.[1,8,12] Though the cytotoxicity is reduced to a large extent by the above ligand exchange process, however, significant differences in biological activities are observed for differently surface modified GNPs. These are mainly due to the chemical properties of the ligand itself or to the enhanced interaction of the GNP with serum proteins in the biological media, forming a protein corona around the GNPs. They are dynamically exchanged with different macromolecules once introduced into the cellular environment.[14,15] This corona extensively influences the target-specific efficient delivery in an actual in vivo environment, proinflammatory effects,[16] and cell-specific uptake.[17] The formation of a protein corona is exclusively dependent on the surface chemistry of the ligands around GNPs.[18] The kinetics of the corona formation can be slowed down by dense grafting of surface ligands or vice versa.[19,20] However, the dependency of grafting of a surface ligand to its hydrophobic chain length and its orientation still remain unclear. Hence, the surface chemistry around the GNP with a minimal toxic effect of ligands along with minimal GNP protein interactions is the prerequisite for improving the cell-specific uptake, targeted drug delivery, and applications in nanomedicine.

A number of techniques such as high-performance liquid chromatography,[21] thermogravimetric analysis,[22] surface plasmon resonance,[23] and fluorescence assay[24] give both qualitative and quantitative estimation of only the surface density of ligand molecules; however, they are beyond typical analytical practices and do not provide information about the relation of chain length to its surface grafting or density.[20,25] Computational simulations, though a very complicated task for the macromolecular assembly onto a GNP surface, can complement the experimental research in an efficient manner.[26]

Here, we present a quantitatively estimated theoretical optimal balance among hydrophobic chain length, the surface density, and charges of the surface ligands for GNP−protein interactions. The main aim of the present study is to see how the orientation and stability of protein binding to a GNP surface are influenced by the surface ligands. To this end, a {111} flat GNP surface (10 nm × 7 nm) mimicking the particle curvature of a GNP (more than 40 nm diameter) was constructed (Figure S1, Supporting Information). The different surface ligands were placed (considering rigid models) on top of the surface. Docking simulation was performed using AutoDock 4.2[27] tools with a semiempirical free-energy force field to evaluate conformations during docking. The chosen computational method and its validation are described in the

Received: September 3, 2013
Accepted: October 18, 2013

   dx.doi.org/10.1021/jz401874u | J. Phys. Chem. Lett. 2013, 4, 3747−3752

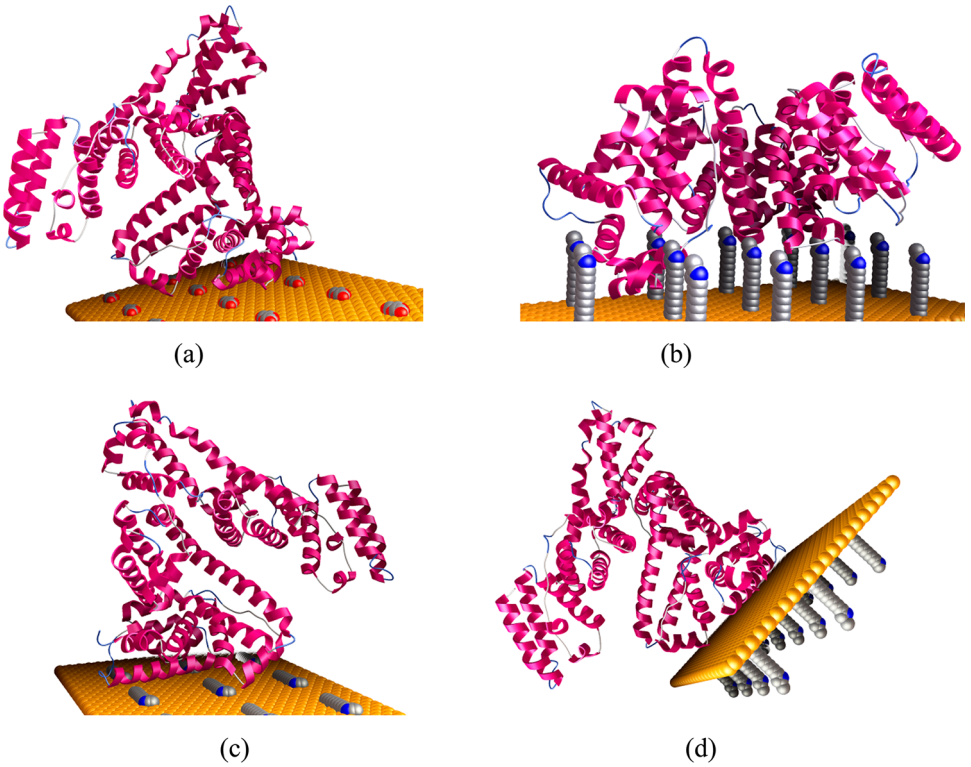

Figure 1. Effect on the protein−GNP interaction upon different surface modification by citrate and different orientations of CTAB. (a) Docking of HSA on a citrate layer with a surface density of 0.25 molecules/nm^2 shows a perpendicular attachment of HSA with its IA domain on the GNP surface. (b) On a CTAB layer (both side covered) with the same surface density, showing a completely different orientation. (c) When the hydrophobic tails of CTAB are laying on the surface, the same orientation as that of citrate layer is observed. (d) Docking of HSA on a single side covered CTAB supports the idea that HSA prefers a flat GNP surface for a comfortable and stable docking. The data suggest that long hydrophobic chains of CTAB hinder the protein docking.

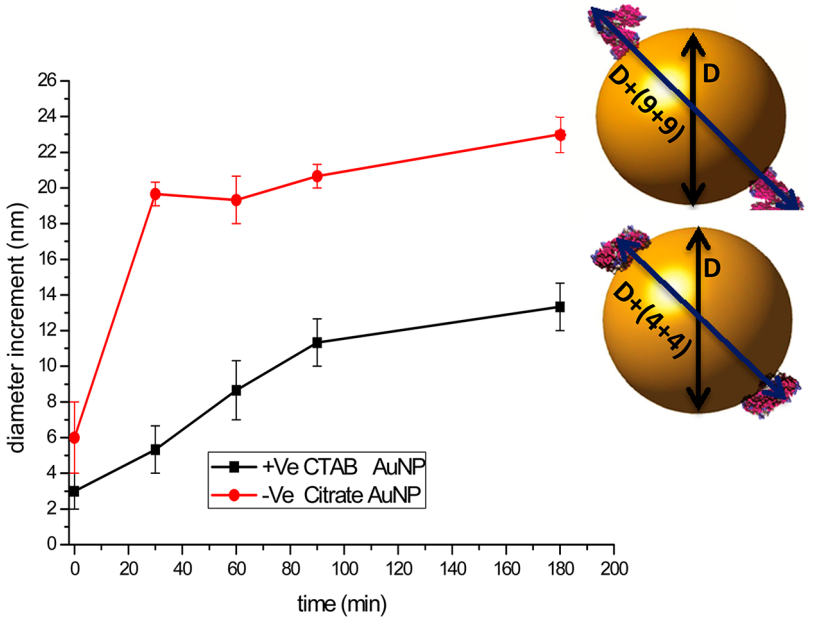

Figure 2. Kinetics of HSA hard corona formation on two different GNPs. DLS data show the fastest kinetics for the citrate-coated GNP and the slowest for the CTAB-coated GNP. The increase in diameter is around 18 nm for citrate−GNP and 8 nm for CTAB−GNP. The inset shows the schematic diagram of the protein binding.

Supporting Information (Figure S2). It is worth mentioning the complexity to match the simulated time scale to the experimental time scale for corona formation. Further, a single protein nanoparticle interaction can never be ideal to provide the kinetics of real corona. However, this novel method was found to be very simple and elegant yet accurate at the same time.[28] CTAB, SDS, and mercapto compounds (acid and amine counter parts) with 6, 12, and 16 alkyl chain lengths were used

dx.doi.org/10.1021/jz401874u | J. Phys. Chem. Lett. 2013, 4, 3747−3752

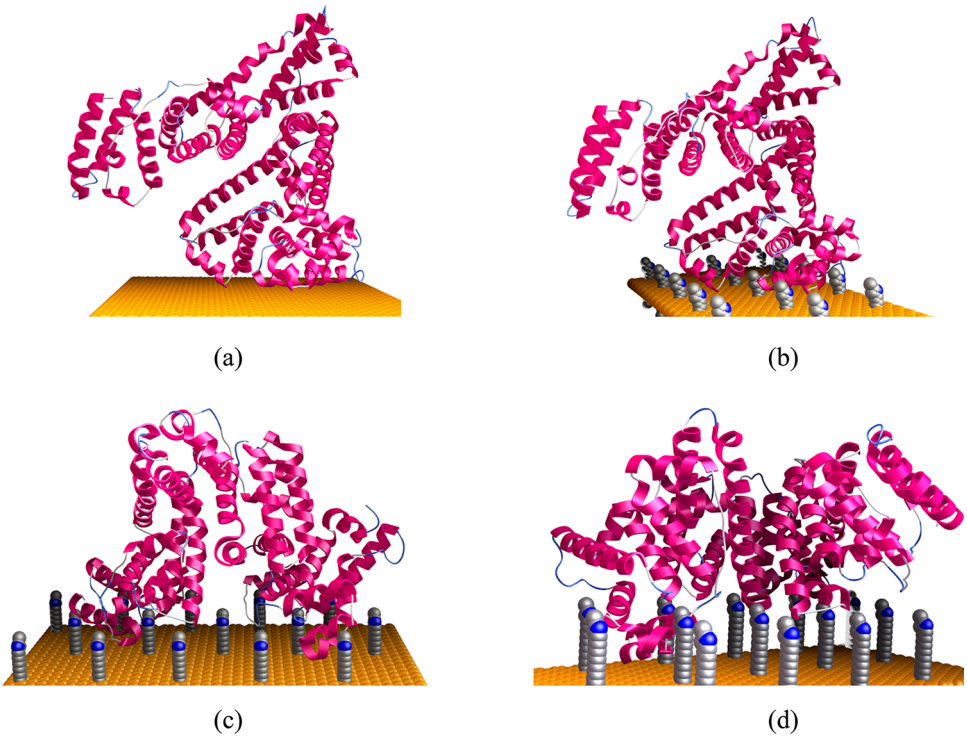

Figure 3. Effect of the hydrophobic chain length on the GNP−protein interaction. Protein−GNP binding on a (a) 0, (b) 6, (c) 12, and (d) 16 alkyl chain length with $-N(CH_3)_3^+Br$ (mimic of CTAB) as the hydrophilic head shows a clear transition from perpendicular to parallel oriented attachment of the protein to the GNP surface.

as surface ligands for a comparative study of the effect of the chain length on protein binding. Hypothetical small PEG molecules $[(OCH_2CH_2)_n$, where n = 2, 3, 5] were also constructed for comparison (Figure S3, Supporting Information). Human serum albumin (HSA) was used as a model protein.

Sodium citrate is the most common reducing agent for synthesizing the spherical GNPs. Hence, as a first step, the docking of HSA protein was performed on a citrate surface with a density of 0.25 molecules/nm^2. HSA was found to dock in a perpendicular orientation with its IA subdomain for the most stable conformation on a citrate surface (Figure 1a). The binding energy is contributed to by a Lennard-Jones potential, the hydrogen bonding energy, and the desolvation energy. The electrostatic interaction was observed not to play much of a role in this case.

A close view of 1 Å resolution shows that the mechanical structure is quite stable as the contacts of 12 amino acid residues of a single long α helix in the center and two other contacts on both sides of it form a crawling-like structure (Table S1 and Figure S4, Supporting Information).

When the CTAB molecule was incorporated on to the GNP surface (CTAB considered as a rigid body and kept perpendicular to the surface with the same surface density as the citrate layer), the docking of protein occurred in a completely different orientation (Figure 1b). Instead of only one α helix (as observed for the citrate layer), multiple helices from different regions were found to attach. The stability of the docking conformation also drastically reduced (Table S2, Supporting Information). However, docking of HSA on a laying CTAB layer (parallel to the gold surface) strikingly keeps a similar docking orientation as that in the citrate layer with almost the same binding energy, suggesting that the orientation of surface ligands plays a very crucial role (Figure 1c). On the other hand, when one side of the surface was covered with CTAB molecules, keeping the other side empty, HSA docked preferably on the bare surface (Figure 1d), suggesting that the long hydrophobic chain really hinders the protein binding.

The above theoretical orientations and hence the effective thickness of the protein layer (protein hard corona) were experimentally verified around 40 nm GNPs (both citrate- and CTAB-coated) using the time-dependent dynamic light scattering (DLS) method (Supporting Information).[14,29] In the citrate-coated GNP, the increment in diameter was very rapid in the first quarter of an hour (Figure 2). However, for the CTAB-coated GNP, the saturation was achieved gradually within 90−120 min. The length of the increased diameter was also approximately 20 nm in citrate-coated GNPs, whereas on a CTAB-coated GNP, it was 8 nm. Simulation results showed that HSA uses its longest possible length, which is around 9 nm, to strongly attach with the citrate-coated surface.

Hence, theoretically, the maximum thickness should be 18 nm (9 nm +9 nm) for a citrate-coated GNP. A CTAB layer on the other hand destabilizes the conformation of HSA, which uses its shorter length (4 nm) to dock on the surface. The thickness in this case will be therefore 8 nm (4 nm + 4 nm), which is very close to the experimental data. Hence, the experimental finding clearly shows the same increase of length and kinetics for the two GNPs, proving that the hard corona is formed as single layer with a specific orientation of the proteins.

Simulation results show a very close relation among the hydrophobic chain length, surface density, and charges on the hydrophilic head of the surfactant molecule with respect to the orientation and stability of the protein. Figure 3a−d shows how the orientation of HSA protein changes from a 0 alkyl hydrophobic chain to a 16 alkyl chain CTAB molecule. A clear

dx.doi.org/10.1021/jz401874u | J. Phys. Chem. Lett. 2013, 4, 3747−3752

transition from perpendicular to parallel orientation of HSA on the GNP surface was observed. It was very evident that a layer of molecules with a short chain length helps the docking process with increased stability. The binding stability starts decreasing with an increasing chain length when the hydrophobic chain length of the CTAB molecule hypothetically changes (Table 1). The same trend was followed for all of the

Table 1. Effect of Hydrophobic Chain Length along with Hydrophilic Head Charges on the GNP−Protein Interaction[a]

chain length	SDS (SO_4^-)	CTAB [$N(CH_3)_3^+$]	COO− (−)	OCH_3 (0)	NH_3^+ (+)	mimic PEG−COOH
6 carbon	−16	−35	−18	−24	−40	−29
12 carbon	−7	−24	−2	−16	−27	−14
16 carbon	−1	−22	+4	−8	−15	−4

[a]The general formula of the five molecules is [SH $(CH_2)_n$X], where X = SO_4^-, $N(CH_3)_3^+$, COO^-, OCH_3, and NH_3^+ and n = 6, 12, and 16. The table shows that the binding stability (kcal/mol) decreases with increasing chain length, irrespective of the hydrophilic head structure. However, for the same length of the carbon chain (hydrophobic tail), the negatively charged hydrophilic molecule shows less stability than the positive counterpart. SDS exhibits much more instability in protein binding compared to CTAB. In the presence of a mimic PEG−COOH [$SH(OCH_2CH_2)_nCOOH$] chain, the stability increases compared to a normal alkyl[$SH(CH_2)_nCOOH$] chain.

surface ligands irrespective of the hydrophobic chemical structure and charges on it. The charges on the top of an alkyl chain can play a very significant role. For example, a layer of modified SDS (negative charge on the hydrophilic head) and a layer of modified CTAB (positive charge on the hydrophilic head) with the same chain length differ significantly in terms of binding energy because of their different architectures and charges on the hydrophilic head. The positive charge on the hydrophilic head favors protein adsorption strongly, while a negative charge hinders the process.

This was also verified with different chemical structures of the hydrophilic head (OMe, COOH, and NH_2). The stability of the five groups is in the following order: $NH_3^+ > N(CH_3)_3^+ > OCH_3 > SO_4^- > COO^-$. For negatively charged surfactant, an optimum alkyl chain length was required for the minimum protein adsorption (with a surface density of 0.25/nm^2). On the other hand, a surfactant molecule with a positive charged head still shows efficient protein binding with the same chain length (Table 1). Recently, the same conclusion was also obtained experimentally using a GNP conjugated with negatively charged 11-mercaptoundecanoic acid (GNP−MUA containing a COOH group) and a GNP conjugated with amino-undecanethiol (GNP−AUT, containing NH_2) as the positive charge, keeping the hydrophobic tail the same. The mercapto modifications on the surface avoid the protein corona formation, while the other counterpart has no effect.[14] Further, mercapto molecules are found to be more effective than a similar length of mimic PEG molecules. The reason behind it is the valuable negative charge on the top, which gets dispersed in the whole PEG molecule as many oxygen atoms are present throughout the chain. It is also likely that intermolecular repulsion will be more in the case of PEG, resulting in difficulties to achieve a close packing compared to that of the mercapto compounds. Our results suggest that the hydrophobic chain length along with the surface density and changes of different types of surface ligands can act as a ruler for the different types of GNP−protein interactions (Table 1).

The docking on different GNP surfaces was also studied for several other serum proteins to get an idea whether the chain length of the surface ligands has a general effect on protein binding and stability. Though each protein (ubiquitin, hemoglobin, insulin, and transferrin) binds to the GNP surface in a unique way, interestingly, they follow the same trend of binding energies in different surfactant layers, as observed in the case of HSA protein (Table 2 and Figures S5−S8, Supporting

Table 2. Comparison of Binding Energies among Five Different Common Human Proteins[a]

proteins	bare surface	citrate layer	CTAB layer	SDS layer
HSA	−36	−41	−22	−7
transferrin	−31	−37	−12	−6
ubiquitin	−27	−30	−18	−15
insulin	−33	−36	−19	−15
hemoglobin	−25	−30	−18	−7

[a]The surface is bare in one case and covered with three different surface modifiers in other cases. The value of the binding energy (kcal/mol) is the highest (most stable) in the case of citrate and the lowest (most unstable) in the case of SDS. All five proteins follow the same trend of energy.

Information). Binding of all of the other proteins was favored on a citrate layer, while the SDS layer was the most unfavorable for docking. This proves our insights regarding chain length and charges not being restricted with only HSA; rather, they might be quite universal for most of the serum proteins.

Apart from the above serum proteins, a larger protein fibrinogen was also docked on the GNP surface. Because the protein was quite larger (45 nm in length and 5 nm in diameter)[16,30] than the surface that we constructed, the docking simulation was performed using specific regions of the proteins. The C-terminal molecular recognition unit of fibrinogen protein was specifically selected for studying its attachment with the gold surface. It was found that two particular docking conformations were very stable. One docks with the end residues, where the gold surface remains perpendicular (end on) to the fibrinogen molecule, and in another case, the surface remains parallel (side on) to the length of fibrinogen (Figure 4a,b). This result is absolutely concordant with the previous model found by experimental work.[30]

Finally, the study aims to enlighten on the role of surface chemistry in nanoparticle protein interactions. In general, a molecule with a larger chain length exhibits more reluctance toward protein adsorption. Mercaptohexadecanoic acid [$SH(CH_2)_{14}COOH$] was found to be better than its positive counterpart ([$SH(CH_2)_{14}NH_2$] or mimic of the PEG molecule [$SH(OCH_2CH_2)_4COOH$]) for minimum protein adsorption on the GNP surface. These results will enrich the field of nanomedicine by providing impetus toward rational design of smarter GNPs for target-specific delivery. This scope of study also could be extended for the site-specific GNP−antibody (IgG) interaction and their binding affinities. Further, the study could be extended to the GNP curvature-dependent molecular insights of GNP−protein interactions.

EXPERIMENTAL METHODS

Nanoparticle Synthesis. Synthesis of the Citrate-Coated GNP (40 nm). Deionized water (36.5 mL) was taken in a conical

dx.doi.org/10.1021/jz401874u | J. Phys. Chem. Lett. 2013, 4, 3747−3752

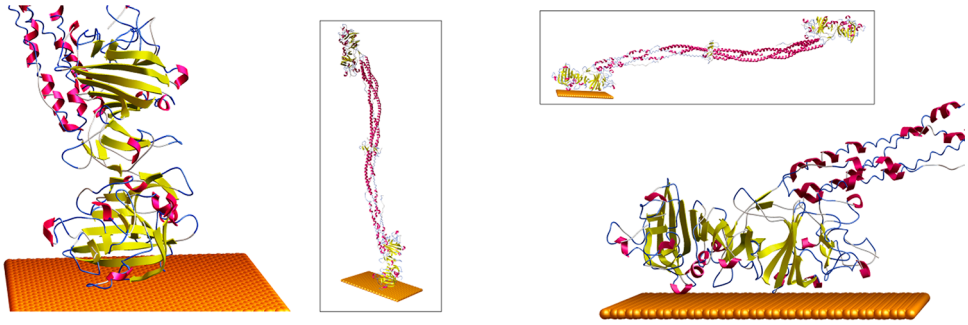

Figure 4. Fibrinogen docking on a {111} flat GNP surface. Two different docking orientations (a) perpendicular and (b) parallel were observed, which nicely matches with the experimental results.[30]

flask, and 0.5 mL of 10 mM $HAuCl_4$ solution was added to it, maintaining the temperature at 40 °C under vigorous stirring on a hot magnetic stirrer. When vapors arose from the solution, 1 mL of a 5 mM aqueous solution of sodium citrate and 1 mL of 50 mM $NaBH_4$ (cold) solutions were added to the solution. The solution was then kept at room temperature and stirred for an additional 10 min until the color of the solution turned from pale yellow to light red. The resulting mixture was aged for 2−4 h to allow the hydrolysis of unreacted $NaBH_4$.

Synthesis of CTAB-Coated GNP (40 nm). The container for seed synthesis held 5 mL of 0.50 mM $HAuCl_4$ and 5 mL of 0.20 M CTAB. The solution was reduced by addition of 600 μL of ice-cold $NaBH_4$ (0.010 M). Next, the container was shaken vigorously for 2 min and occasionally opened. The seed solution was a brown suspension and was allowed to age for 2 h. CTAB-coated spherical GNPs were prepared by adding 12 μL of seed to a solution containing 9.50 mL of 0.10 M CTAB, 80 μL of 0.010 M $AgNO_3$, 500 μL of 0.010 M $HAuCl_4$, and 55 μL of 0.10 M ascorbic acid. This mixture was also stirred for 10 s, which resulted in a red suspension that was again left undisturbed for 24 h to increase the yield.

Nanoparticle Characterization. DLS Measurement. The hydrodynamic radii of the GNPs were measured using dynamic light scattering (DLS) using a Zetasizer Nano equipped with He Ne laser illumination at 633 nm and a single-photon counting avalanche photodiode for signal detection (Malvern Instrument). The autocorrelation function was performed by an ALV-5000/EPP photon correlator (ALV, Langen, Germany) and analyzed using Dispersion Technology Software (DTS) (Malvern Instruments). A volume of the 3 mL of the colloidal solution of the GNP was placed into a specific cuvette (as suggested). The refractive index, absorption coefficient, viscosity of the solvent, and temperature (20 °C) were provided by the software. For each sample, the autocorrelation function was the average of five runs of 10 s each.

Transmission Electron Microscopy. The particle size and dispersity of the synthesized nanoparticles were obtained using a TECNAI 200 kV TEM (FEI, Electron Optics) electron microscope with 200 kV input voltage (Figure S9, Supporting Information). TEM grids were prepared by placing 5 μL of a diluted and well-sonicated sample solution on a carbon-coated copper grid and evaporating the solution at room temperature completely. Contamination from various sources like dust particles and the glassware was taken care of very carefully.

Monitoring the Kinetics of HSA Hard Corona. To monitor the kinetics of hard and soft corona formation around GNPs, a DLS experiment was performed with respect to time. For time-dependent protein-associated GNP measurements, the GNP (0.64 nM) and protein (10 μM) in phosphate buffer (pH 7.4) were incubated at room temperature. Centrifugation is a very efficient and reliable way to segregate particle-associated proteins from nonassociated protein.[4,28] Centrifugation was performed for the separation of loosely bound or unbound protein at each time interval immediately after the measurement of the hydrodynamic radii on that particular time interval. After incubation of the GNP with protein, the solution was centrifuged for approximately 10 min at 10000*g* followed by pellet resuspension in an equal amount of exchanged solvent (water).

■ ASSOCIATED CONTENT

Supporting Information

Details of surface construction, docking experiments, protocols, supporting figures, and supporting tables. This material is available free of charge via the Internet at http://pubs.acs.org.

■ AUTHOR INFORMATION

Corresponding Author

*E-mail: chayan@iitmandi.ac.in.

Notes

The authors declare no competing financial interest.

■ ACKNOWLEDGMENTS

The authors acknowledge the home institute (IIT Mandi) and Department of Science and Technology (DST) India for their financial support (Project No: IITM/SG/CKN/003 and SR/FT/CS-152/2011) for running the docking simulations and experiments. The authors acknowledge the All India Institute of Medical Sciences (AIIMS), New Delhi, India for using their TEM facility.

■ REFERENCES

(1) Grabinski, C.; Schaeublin, N.; Wijaya, A.; Couto, S. H.; Baxamusa, K.; Schifferli, H.; Hussain, S. M. Effect of Gold Nanorod Surface Chemistry on Cellular Response. *ACS Nano* **2011**, *5*, 2870−2879.

(2) Arvizo, R. R.; Miranda, O. R.; Thompson, M. A.; Pabelick, C. M.; Bhattacharya, R.; Robertson, J. D.; Rotello, V. M.; Prakash, Y. S.; Mukherjee, P. Effect of Nanoparticle Surface Charge at the Plasma Membrane and Beyond. *Nano Lett.* **2010**, *10*, 2543−2548.

(3) Cho, E. C.; Zhang, L.; Au, Q.; Xio, Y. The Effects of Size, Shape and Surface Functional Group of Gold Nanostructures on Their Adsorption and Internalization by Cells. *Small* **2010**, *6*, 517−522.

(4) Hong, R.; Han, G.; Fernandez, J. M.; Kim, B. J.; Forbes, N. S.; Rotello, V. M. Glutathione-Mediated Delivery and Release Using

Monolayer Protected Nanoparticle Carriers. *J. Am. Chem. Soc* . **2006**, *128*, 1078−1079.
(5) Nativo, P.; Prior, I. A.; Brust, M. Uptake and Intracellular Fate of Surface-Modified Gold Nanoparticles. *ACS Nano* **2008**, *2*, 1639−1644.
(6) Oyelere, A. K.; Chen, P. C.; Huang, X. H.; El-Sayed, I. H.; El-Sayed, M. A. Peptide-Conjugated Gold Nanorods for Nuclear Targeting. *Bioconjugate Chem.* **2007**, *18*, 1490−1497.
(7) Verma, A.; Stellacci, F. Effect of Surface Properties on Nanoparticle−Cell Interactions. *Small* **2010**, *6*, 12−21.
(8) Liang, M.; Lin, I.; Whittaker, M. R.; Minchin, R. F.; Monteiro, M. J.; Toth, I. Cellular Uptake of Densely Packed Polymer Coatings on Gold Nanoparticles. *ACS Nano* **2010**, *4*, 403−413.
(9) Loo, C.; Lowery, A.; Halas, N. J.; West, J.; Drezek, R. Immuno Targeted Nano Shells for Integrated Cancer Imaging and Therapy. *Nano Lett.* **2005**, *5*, 709−711.
(10) Au, L.; Zheng, D. S.; Zhou, F.; Xia, Z. Y.; Li, X. D.; Li, Y. N. A Quantitative Study on the Photothermal Effect of Immuno Gold Nanocages Targeted to Breast Cancer Cells. *ACS Nano* **2008**, *2*, 1645−1652.
(11) Millstone, J. E.; Hurst, S. J.; Metraux, G. S.; Cutler, J. I.; Mirkin, C. A. Colloidal Gold and Silver Triangular Nanoprisms. *Small* **2009**, *5*, 646.
(12) Bartneck, M.; Keul, H. A.; Singh, S.; Czaja, K.; Bornemann, J.; Bockstaller, M.; Moeller, M.; Zwadlo-Klarwasser, G. Rapid Uptake of Gold Nanorods by Primary Human Blood Phagocytes and Immunomodulatory Effects of Surface Chemistry. *ACS Nano* **2010**, *4*, 3073−3086.
(13) Vigderman, L.; Manna, P.; Zubarev, E. R. Quantitative Replacement of Cetyltrimethylammonium Bromide by Cationic Thiol Ligands on the Surface of Gold Nanorods and Their Extremely Large Uptake by Cancer Cells. *Angew. Chem., Int. Ed.* **2012**, *51*, 636−641.
(14) Casals, E.; Pfaller, T.; Duschl, T.; Oostingh, G. J.; Puntes, V. Time Evolution of the Nanoparticle Protein Corona. *ACS Nano* **2010**, *4*, 3623−3632.
(15) Lundqvist, M.; Stigler, J.; Elia, G.; Lynch, I.; Cedervall, T.; Dawson, K. A. Nanoparticle Size and Surface Properties Determine the Protein Corona with Possible Implications for Biological Impacts. *Proc. Natl. Acad. Sci. U.S.A.* **2008**, *105*, 14265−14270.
(16) Salvati, A.; Pitek, A. S.; Monopoli, M. P.; Prapainop, K.; Bombelli, F. B.; Hristov, D. R.; Kelly, P. M.; Aberg, C.; Mahon, E.; Dawson, K. A. Transferrin-Functionalized Nanoparticles Lose Their Targeting Capabilities when a Biomolecule Corona Adsorbs on the Surface. *Nat. Nanotechnol.* **2013**, *8*, 137−143.
(17) Lesniak, A.; Campbell, A.; Monopoli, M. P.; Lynch, I.; Salvati, A.; Dawson, K. A. Serum Heat Inactivation Affects Protein Corona Composition and Nanoparticle Uptake. *Biomaterials* **2010**, *36*, 9511−9518.
(18) Xia, X.; Yang, M.; Wang, Y.; Zheng, Y.; Chen, Q.; Li, J.; Xia, Y. Quantifying the Coverage Density of Poly(ethylene glycol) Chains on the Surface of Gold Nanostructures. *ACS Nano* **2012**, *6*, 512−522.
(19) Nichols, J. W.; Bae, Y. H. Odyssey of a Cancer Nanoparticle: From Injection Site to Site of Action. *Nano Today* **2012**, *7*, 606−618.
(20) Perry, J. L.; Reuter, K. G.; Kai, M. P.; Herlihy, K. P.; Jones, S. W.; Luft, J. C.; Napier, M.; Bear, J. E.; DeSimone, J. M. PEGylated PRINT Nanoparticles: The Impact of PEG Density on Protein Binding, Macrophage Association, Biodistribution, and Pharmacokinetics. *Nano Lett.* **2012**, *12*, 5304−5310.
(21) Li, S. D.; Huang, L. Nanoparticles Evading the Reticulo Endothelial System: Role of the Supported Bilayer. *Biochim. Biophys. Acta* **2009**, *1788*, 2259−2266.
(22) Cheng, T. L.; Chuang, K. H.; Chen, B. M.; Roffler, S. R. Analytical Measurement of PEGylated Molecules. *Bioconjugate Chem.* **2012**, *23*, 881−899.
(23) Bhattacharya, R.; Patra, C. R.; Earl, A.; Wang, S.; Katarya, A.; Lu, L.; Kizhakkedathu, J. N.; Yaszemski, M. J.; Greipp, P. R.; Mukhopadhyay, D.; Mukherjee, P. Attaching Folic Acid on Gold Nanoparticles using NonCovalent Interaction via Different Polyethylene Glycol Backbones and Targeting of Cancer Cells. *Nanomedicine* **2007**, *3*, 224−238.
(24) Jokerst, J. V.; Lobovkina, T.; Zare, R. N.; Gambhir, S. S. Nanoparticle PEGylation for Imaging and Therapy. *Nanomedicine* **2011**, *6*, 715−728.
(25) Makrodimitris, K.; Masica, D. L.; Kim, E. T.; Gray, J. J. Structure Prediction of Protein−Solid Surface Interactions Reveals a Molecular Recognition Motif of Statherin for Hydroxyapatite. *J. Am. Chem. Soc.* **2007**, *129*, 13713−13722.
(26) Brancolini, G.; Kokh, D. B.; Calzolai, L.; Wade, R. C.; Corni, S. Docking of Ubiquitin to Gold Nanoparticles. *ACS Nano* **2012**, *6*, 9863−9878.
(27) Morris, G. M.; Huey, R.; Lindstrom, W.; Sanner, M. F.; Belew, R, K.; Goodsell, D. S.; Olson, A. J. AutoDock4 and AutoDockTools4: Automated Docking with Selective Receptor Flexibility. *J. Comput. Chem.* **2009**, *30*, 2785−2791.
(28) Monopoli, M. P.; Aberg, C.; Salvati, A.; Dawson, K. A. Biomolecular Coronas Provide the Biological Identity of Nanosized Materials. *Nat. Nanotechnol.* **2012**, *7*, 779−786.
(29) Cedervall, T.; Lynch, I.; Foy, M.; Berggård, T.; Donnelly, S. C.; Cagney, G.; Linse, S.; Dawson, K. A. Detailed Identification of Plasma Proteins Adsorbed on Co-Polymer Nanoparticles. *Angew. Chem., Int. Ed.* **2007**, *46*, 5754−5756.
(30) Deng, Z. J.; Liang, M.; Toth, I.; Monteiro, M. J.; Minchin, M. Molecular Interaction of Poly(acrylic acid) Gold Nanoparticles with Human Fibrinogen. *ACS Nano* **2012**, *6*, 8962−8969.